

A Scaling Relationship for Satellite-Forming Impacts

Robin M. Canup and William R. Ward

Department of Space Studies, Southwest Research Institute, 1050 Walnut Street, Boulder, Colorado 80302

E-mail: robin@boulder.swri.edu

and

A. G. W. Cameron

Lunar and Planetary Laboratory, University of Arizona, Tucson, Arizona 85721

Received July 19, 2000; revised November 22, 2000

We describe a scaling relationship that can be used to characterize the results of numerical smooth particle hydrodynamic (SPH) experiments of potential satellite-forming impacts. The relationship is used to interpret and summarize data from 41 such SPH simulations, all employing an impactor-to-target mass ratio of 3:7, but with a variety of total masses and angular momenta. The results can be utilized to infer other classes of impacts beyond those simulated to date that are plausible Moon-forming candidates.

© 2001 Academic Press

Key Words: Moon; impact processes; planetary formation; satellites; accretion.

INTRODUCTION

The current leading theory for the formation of the Moon is the giant impact hypothesis (Hartmann and Davis 1975, Cameron and Ward 1976). This theory proposes that during the final stages of its accretion, protoearth suffered a collision with another protoplanetary body, leaving debris in orbit about the Earth from which the Moon then accumulated. Cameron and co-workers (e.g., Cameron and Benz 1991, Cameron 1997, 2000a,b) have performed numerous smooth particle hydrodynamic (SPH) calculations intended to simulate potential moon-forming impact events. These simulations have considered a variety of impact angular momenta, as well as combined impactor and protoearth masses.

While early simulations (Benz *et al.* 1986, 1987, 1989, Cameron and Benz 1991) modeled the protoearth and impactor with only a few thousand SPH particles (such that a lunar mass worth of ejected debris was represented by only a few tens of particles), recent works have utilized between $N = 10,000$ and 100,000 total particles (Cameron 1997, 2000a,b) allowing for a better resolution of ejected material. Here the results of 41 impact simulations performed by Cameron are compiled, includ-

ing 35 simulations utilizing $N = 10,000$ particles, 3 utilizing $N = 20,000$, and 3 utilizing $N = 100,000$ particles. The simulations all employed the equation of state known as ANEOS (as described in Benz *et al.* (1989)) and assumed an impact velocity equal to the mutual escape velocity of the protoearth and impactor. Both the total system mass, M_T , and the angular momentum of the colliding pair, L , were varied. Impactor and target bodies were assumed to be composed of silicate mantles and iron cores. Table I lists the data from these simulations. Figures 1a and b show the total mass of debris placed into bound orbit (in lunar masses) and the angular momentum of this debris, both as functions of L normalized to the current angular momentum of the Earth–Moon system, $L_{EM} = 3.5 \times 10^{41} \text{ g} \cdot \text{cm}^2/\text{s}$. Appendix A describes the basic method used to calculate these quantities from the output of a given SPH simulation.

A prevailing trait of the simulation results is an apparent difficulty in placing a sufficient amount of mass into orbit to yield the Moon for a total system mass and impact angular momentum equal to that of the current Earth–Moon system (e.g., Cameron 1997, 2000a,b, Cameron and Canup 1998). Models of the accumulation of the Moon from an impact-generated disk suggest that an initial disk mass of at least two lunar masses, or a disk with a lunar mass of material exterior to the Earth's Roche limit,¹ is required to yield the Moon (Canup and Esposito 1996, Ida *et al.* 1997). One class of impact that appears capable of producing sufficiently massive disks includes those involving a total mass equal to that of the Earth and Moon ($M_T = M_{EM}$) and an impact angular momentum significantly greater than that of the current Earth–Moon system, or $L \sim 2L_{EM}$. Interactions of the Earth–Moon system with the Sun act to decrease the system angular momentum, although this likely resulted in only a

¹ For lunar density materials, $a_{Roche} = 2.9R_{\oplus}$.

TABLE I
Data from SPH Giant Impact Experiments by Cameron (2000a)

Total mass M_T/M_\oplus	Col. A.M. L/L_{EM}	Disk mass M_D/M_{moon}	Disk A.M. L_d/L_{EM}	Col. A.M. L/L_*	Disk mass M_D/M_T	Disk A.M. L_d/L_*
● 0.50	0.500	0.26	0.0327	0.545	0.0064	0.0357
0.50	0.625	0.60	0.0832	0.682	0.0148	0.0908
0.50	0.750	1.16	0.178	0.818	0.0285	0.194
0.50	0.811	1.36	0.218	0.885	0.0335	0.238
0.50	0.874	1.62	0.259	0.954	0.0399	0.283
0.50	0.936	1.41	0.228	1.021	0.0347	0.249
● 0.55	1.00	2.09	0.323	0.931	0.0467	0.301
0.55	1.25	1.41	0.219	1.163	0.0315	0.204
● 0.60	1.00	1.32	0.228	0.805	0.0271	0.184
0.60	1.25	1.59	0.294	1.006	0.0326	0.237
● 0.65	1.00	1.14	0.163	0.705	0.0216	0.115
0.65	1.05	0.76	0.116	0.740	0.0144	0.082
0.65	1.20	1.84	0.290	0.845	0.0348	0.204
0.65	1.25	1.34	0.279	0.881	0.0254	0.197
▲ 0.65	1.15	1.53	0.268	0.810	0.0290	0.189
0.65	1.20	1.89	0.306	0.845	0.0358	0.216
■ 0.65	1.10	1.60	0.250	0.775	0.0303	0.176
0.65	1.15	1.40	0.219	0.810	0.0265	0.154
0.65	1.20	2.08	0.328	0.845	0.0394	0.231
● 0.70	1.00	0.47	0.080	0.623	0.0083	0.050
▲ 0.70	1.00	0.92	0.140	0.623	0.0162	0.087
0.70	1.10	0.92	0.144	0.685	0.0162	0.090
0.70	1.15	0.95	0.149	0.716	0.0167	0.093
0.70	1.20	1.76	0.262	0.747	0.0309	0.163
0.70	1.25	1.56	0.272	0.778	0.0274	0.169

Table I—Continued

● 0.75	1.00	0.62	0.086	0.555	0.0102	0.048
0.75	1.25	0.91	0.155	0.694	0.0149	0.086
● 0.80	0.80	0.02	0.003	0.399	0.0003	0.001
0.80	1.00	0.43	0.074	0.498	0.0066	0.037
0.80	1.25	0.74	0.124	0.623	0.0114	0.062
● 0.90	1.00	0.06	0.005	0.410	0.0008	0.002
0.90	1.25	0.50	0.088	0.512	0.0068	0.036
● 1.00	1.00	0.07	0.010	0.344	0.0009	0.003
1.00	1.25	0.06	0.010	0.430	0.0007	0.003
1.00	1.50	0.41	0.097	0.515	0.0050	0.033
1.00	1.75	0.35	0.064	0.601	0.0043	0.022
1.00	2.00	1.46	0.278	0.687	0.0178	0.096
1.00	2.25	1.95	0.456	0.773	0.0240	0.157
1.00	2.50	2.44	0.596	0.859	0.0300	0.205
1.00	2.75	3.18	0.777	0.945	0.0391	0.267
1.00	3.00	3.22	0.692	1.031	0.0396	0.238

Note. Symbol colors vary with the total colliding mass, M_T . Circles, triangles, and squares correspond to simulations with $N = 10,000, 20,000,$ and $100,000$ particles, respectively. All entries following a given symbol have the same values of M_T and N .

few percent change.² The only known way to remove a more substantial angular momentum excess subsequent to lunar formation would be a later large impact to the Earth, which would then presumably also add significant mass to the system, making the original assumption of $M_T = M_{EM}$ in this case somewhat inconsistent.

If a smaller total mass is considered for a set impactor to target mass ratio, greater yields of orbiting material are achieved for given impact angular momenta. Simulations have been performed for various values of the total mass ranging from 0.5 to 1 M_{EM} and, in particular, yield disks of sufficient mass to produce the Moon when $M_T \sim 0.65 M_{EM}$ and $L \sim L_{EM}$. Smaller total mass values could be appropriate if the lunar-forming im-

pact occurred before the Earth's accretion was complete (e.g., Cameron and Canup 1998), which is not inconsistent with recent simulations of late-stage terrestrial planet formation that find that the largest impact a planet experiences often occurs prior to the end of its final accretion (Agnor *et al.* 1999). In addition, an “early-Earth” impact may more easily account for the observed tungsten isotopic compositions of the Earth and Moon (e.g., Halliday *et al.* 2000). However, requiring that a significant fraction of the Earth's mass be accreted subsequent to lunar formation may also be problematic. The accretion of $\sim 0.35 M_{EM}$ to the Earth would likely have involved subsequent large impacts, which could significantly alter the angular momentum of the Earth–Moon system and weaken the rationale for assuming the lunar-forming impact occurred with $L \sim L_{EM}$. It also has yet to be demonstrated that the Moon could avoid contamination by siderophile-rich material during the period when the Earth was accumulating the final $\sim 35\%$ of its mass (e.g., Stewart 2000). We note however that the post-impact protoearth probably had an extensive magma ocean, whose larger rate of tidal dissipation may have reduced the period of maximum exposure of the Moon to the gravitationally focused rain of planetesimals onto the protoearth.

²The tidal torque resulting from tides raised on the Earth by the Sun slows Earth's angular spin by a rate $\dot{\omega}_{\oplus} = (3/2K)(k_{2\oplus}/Q_{\oplus})(M_S/M_{\oplus})(R_{\oplus}/a_{\oplus})^3 GM_S/a_{\oplus}^2$, where $k_{2\oplus}$ and Q_{\oplus} are the Earth's Love number and tidal dissipation factor, a_{\oplus} is the Earth's orbital radius, M_S is the solar mass, and $K = 0.335$ is the terrestrial gyration constant. For a fully formed protoearth and a $(k_{2\oplus}/Q_{\oplus})$ value equal to the average required for the Moon to evolve to its current position in 4.5 billion years, $\dot{\omega}_{\oplus} \approx 4 \times 10^{-23}$ rad/s², giving $\Delta\omega = 6 \times 10^{-6}$ rad/s in 4.5 billion years. This decrease represents a fractional change in the Earth–Moon system's angular momentum of $(KM_{\oplus}R_{\oplus}^2\Delta\omega)/L_{EM} \sim 1\%$.

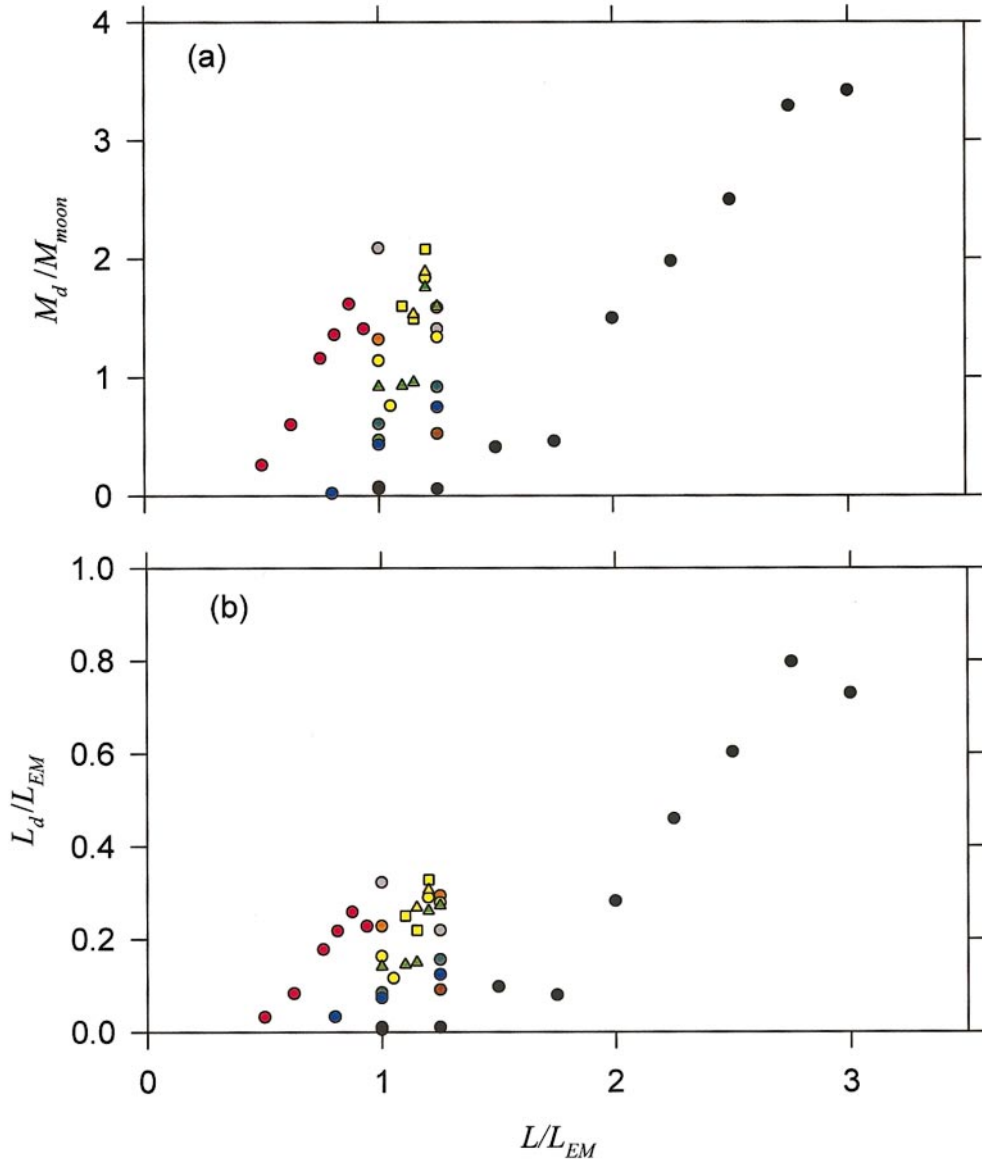


FIG. 1. (a) Disk mass vs. impact angular momentum in units of lunar masses and the angular momentum of the Earth–Moon system. (b) Disk angular momentum vs. impact angular momentum. The symbols and color codes are keyed to the data presented in Table I.

SCALING RELATIONSHIP

An open question is whether there exist classes of impacts intermediate to those described above which could also yield the Moon but would require a more moderate subsequent modification of the mass or angular momentum of the Earth–Moon system. To address this issue, it is useful to employ a scaling law to help characterize and interpret the results of numerical SPH experiments of potential satellite-forming impacts. This relationship can be then used to infer other classes of impacts that are likely Moon-forming candidates. While we have used data produced by models of the lunar-forming event, the relationships derived here may be applicable to other impact-related phenomena as well.

We take as normalization values the total mass, M_T , involved in the collision and the angular momentum of an object containing the total mass of the system spinning at the maximum rate for rotational stability, with the latter obtained by setting the centrifugal force equal to the gravitational force for a spherical solid body, i.e.,

$$L_* = K M_T R_T^2 \sqrt{G M_T / R_T^3} = M_T^{5/3} K \sqrt{G} [3 / (4\pi\rho)]^{1/6}, \quad (1)$$

where K is the gyration constant of a body of mass M_T ($K = 2/5$ for a sphere of uniform density), and ρ is its solid body density. For the Earth, $K = 0.335$, $\rho = 5.6 \text{ g/cm}^3$, and the reference variable reads $L_* = 1.02 \times 10^{42} (M_T / M_\oplus)^{5/3} \text{ g} \cdot \text{cm}^2/\text{s}$.

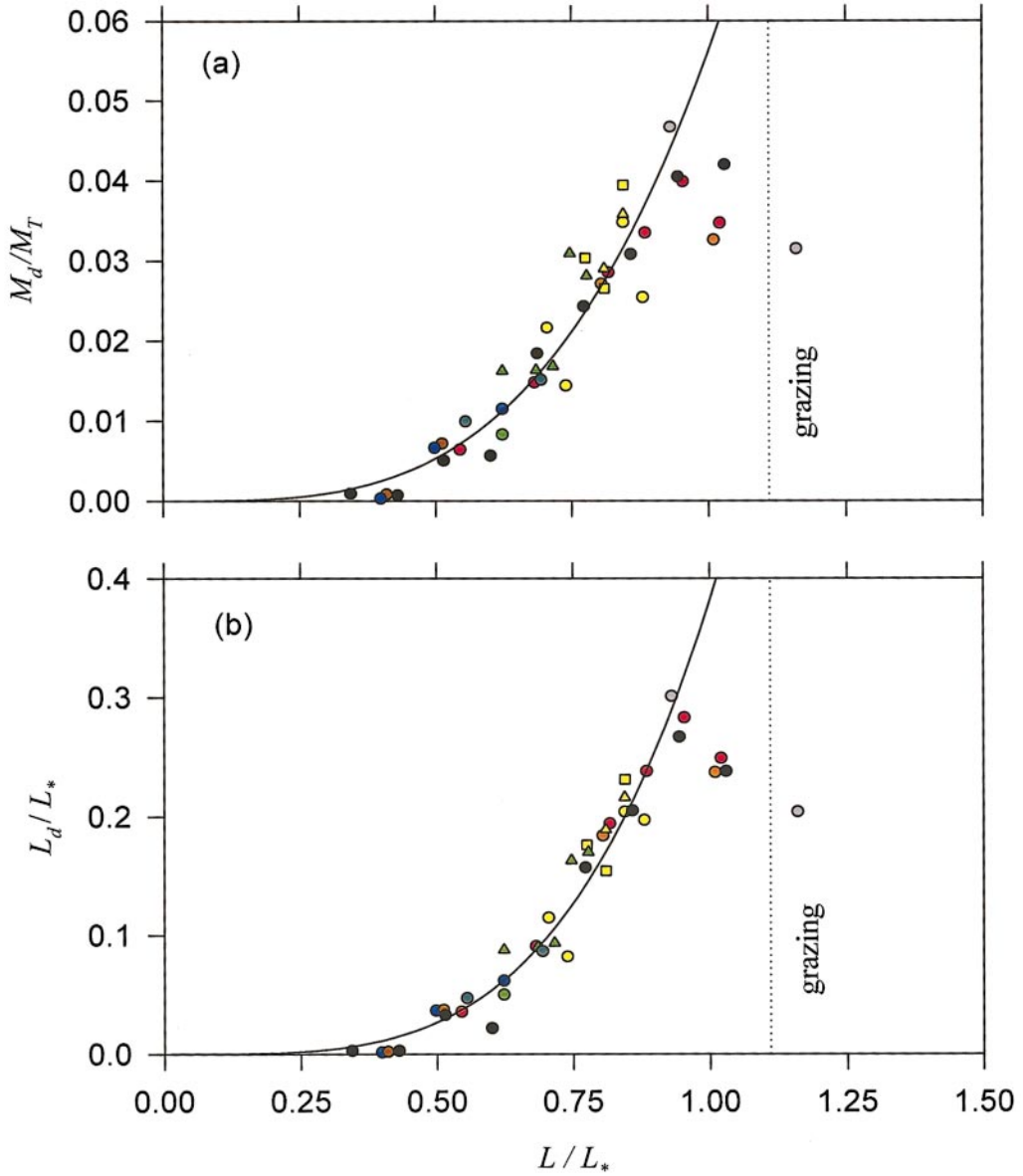


FIG. 2. (a) Disk mass vs. impact angular momentum in units of the total mass and the quantity L_* . The dotted line indicates the limit of a grazing impact for two spherical bodies. Collisions are still possible with impact parameters just beyond this limit owing to tidal distortion upon close approach. (b) Disk angular momentum vs. impact angular momentum in units of L_* . The solid curves in (a) and (b) are power-law fits to data with $0.5 < L/L_* < 1.00$.

The data shown in Table I have been renormalized by dividing the masses and angular momenta by $M_T/M_{Moon} = 81.3(M_T/M_\oplus)$ and $L_*/L_{EM} = 2.91(M_T/M_\oplus)^{5/3}$, respectively. The renormalized data are plotted in Fig. 2. The behavior seen in these frames can be better understood by noting that since all of the simulations here considered the same impactor to target mass ratio, L/L_* is a proxy for the impact parameter, p . For $\sin \xi < 1$, $p = (R_M + R_m) \sin \xi$, where ξ is the angle of the trajectory to the local surface normal (i.e., obliqueness) and R_M and R_m are the radii of the target and projectile, respectively.

Assuming zero energy at infinity (see Appendix B), we have

$$\frac{L}{L_*} = \frac{\sqrt{2}}{K} f(\gamma) \sin \xi, \quad (2)$$

where $\gamma \equiv m/M_T$ is the ratio of projectile mass to the total mass and $f(\gamma) \approx \gamma(1-\gamma)\sqrt{\gamma^{1/3} + (1-\gamma)^{1/3}}$. For all data in Table I, $\gamma = 0.3$ and $f(\gamma) = 0.262$. A grazing impact occurs here for $L/L_* = \sqrt{2}f/K = 1.11$; this boundary is shown as a vertical dotted line in Figs. 2a and b. Still larger values

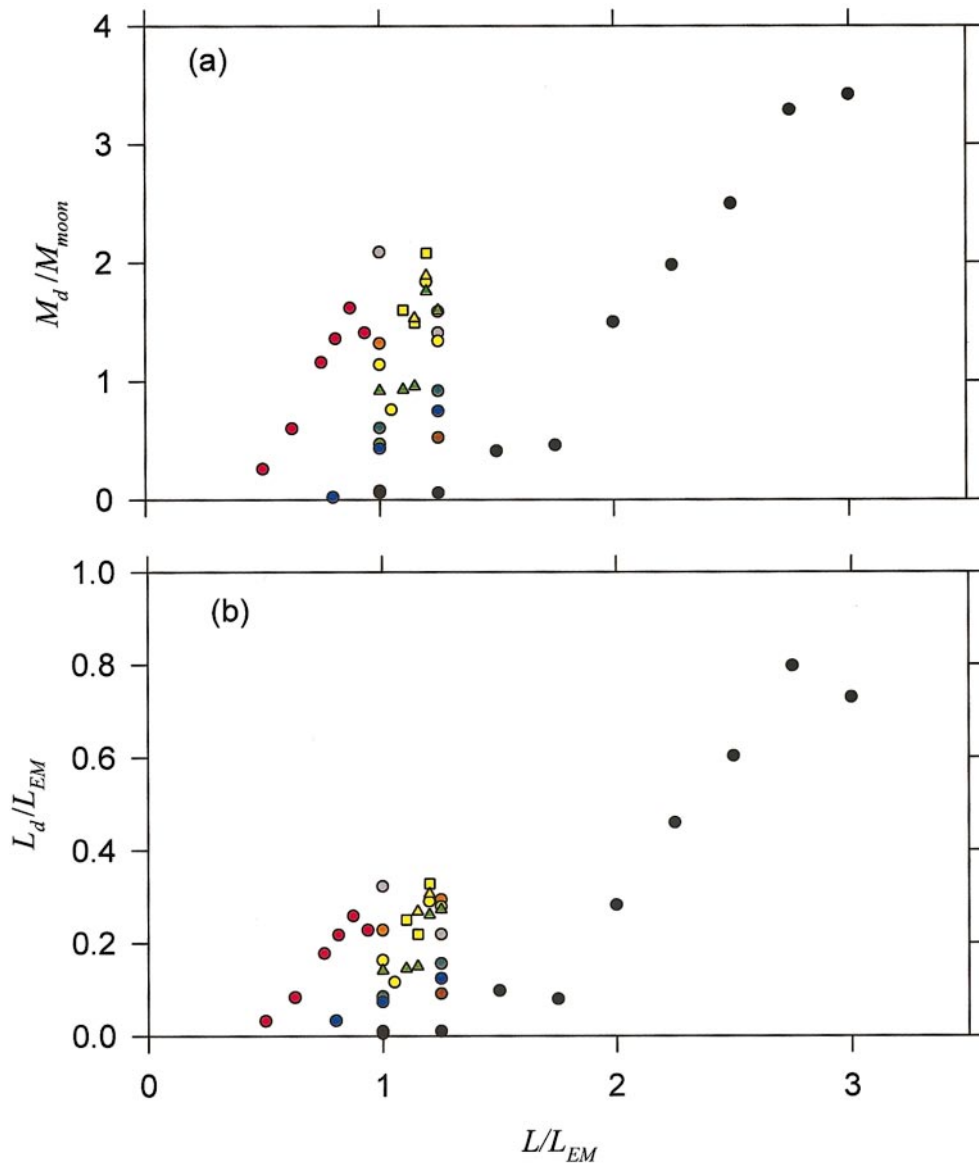


FIG. 3. The mass fraction of iron in the disk vs. (L/L_*) . The dot-dashed curve is approximately the upper limit on the mass fraction of iron in the Moon. One point, corresponding to the simulation with $M_T = 0.55M_{EM}$ and $L/L_* = 1.163$, falls well outside the plotted range and is indicated by the upward arrow; the disk in this run contained 30% iron by mass, or approximately the assumed bulk composition of the impacting body.

of L cause the projectile to miss the target.³ As the impact parameter (and therefore the impact angular momentum) increases and the collision becomes more oblique, the mass yield of orbiting debris goes up. For a given angular momentum, decreasing M_T allows for a larger impact parameter resulting in an increased yield. However, eventually the impact site approaches the edge of the target and the yield of bound orbiting material drops. As this occurs, the amount of material es-

caping the system (less than $0.05M_T$ for the simulations here) increases.

Figure 3 shows the disk mass fraction contained in iron as a function of the scaled impact angular momentum; this fraction generally increases with (L/L_*) . One data point, corresponding to the simulation with $M_T = 0.55M_{EM}$ and $L/L_* = 1.163$, falls well outside the plotted range; the disk in this run contained 30% iron by mass, or approximately the same assumed bulk composition for the impactor. The horizontal dot-dashed line in Fig. 3 is a disk containing 4% iron by mass, corresponding approximately to the upper limit for the mass of the lunar core (e.g., Hood and Zuber 2000). Six out of 7 cases simulated with $(L/L_*) > 0.9$

³ Owing to deformations of target and projectile, collision still occurs for impact parameters slightly greater than $R_M + R_m$.

and 1 out of 34 cases with $(L/L_*) < 0.9$ fall above this limit. Extremely oblique impacts appear to typically produce disks that are too iron-rich to yield the Moon, assuming that a moon would accrete amounts of silicate and iron proportional to the ratio of these elements in the initial disk. However, we note that the amount of disk iron is not well resolved by these simulations (since 1% of a lunar mass is represented by only a few tens of particles even in the $N = 100,000$ runs), and it not clear to what extent the orbiting iron is well mixed throughout the disk.

For convenience, the data in the range $0.5 < L/L_* < 1.00$ in Fig. 2a have been fit (solid curve) by a power law of the form $M_d/M_T = C_M(L/L_*)^{s_M}$ with $C_M = 0.056$, $s_M = 3.40$; those in Fig. 2b have been fit by a power law of the form $L_d/L_* = C_L(L/L_*)^{s_L}$ with $C_L = 0.381$, $s_L = 3.83$. Data above this range begin to show the steep decline associated with the target’s edge; data below this range have too little disk mass to be resolved reliably by the SPH simulations. A lower limit on (L/L_*) needed to yield a long-lived satellite can be found by requiring that the co-rotation radius is interior to the Roche limit, so that any impact-generated satellite that accretes exterior to a_{Roche} will initially evolve outward as the result of tidal interaction with the planet. This yields

$$\frac{L}{L_*} \geq \left[\frac{R_p}{a_R} \right]^{3/2} + \frac{M_M}{KM_T} \sqrt{\frac{a_M}{R_p}}, \quad (3)$$

where ρ_M and ρ_p are the densities of the satellite and planet, and the Roche limit is defined as $a_{Roche} \equiv 2.456(\rho_p/\rho_M)^{1/3} R_p$, where R_p is the planet radius. Equation (3) assumes $M_T \sim M_p$; with $a_M = 1.2a_{Roche}$ and Earth–Moon densities, Eq. (3) yields $(L/L_*) \geq 0.27$.

The power-law representations shown in Figs. 2a and b can be utilized to estimate the total collision mass and impact angular momentum required to yield a given mass and angular momentum disk. Given these, an estimate can be made for the mass of the resulting moon that would accrete from such a disk via conservation of angular momentum (Ida *et al.* 1997). Assuming that the disk material accretes into a single satellite on a circular orbit with semimajor axis a_M , while the remaining disk material accretes onto the Earth, gives

$$M_M = \left[KC_L \left(\frac{L}{L_*} \right)^{s_L} - C_M \left(\frac{L}{L_*} \right)^{s_M} \right] \frac{M_T}{\sqrt{a_M/R_p} - 1}. \quad (4)$$

Accretion simulations (Ida *et al.* 1997, Kokubo *et al.* 2000a,b) find accreted moon masses that agree fairly well with this estimate for disks with most of their mass initially within the Roche limit. For more radially extended disks, a significant fraction of the disk material escapes during the accretion process, so that the resulting moon mass is typically about 20% less than that implied by Eq. (4).

Figure 4 shows contours of the predicted mass of the moon from Eq. (4) (in lunar masses) that would accrete from impact-

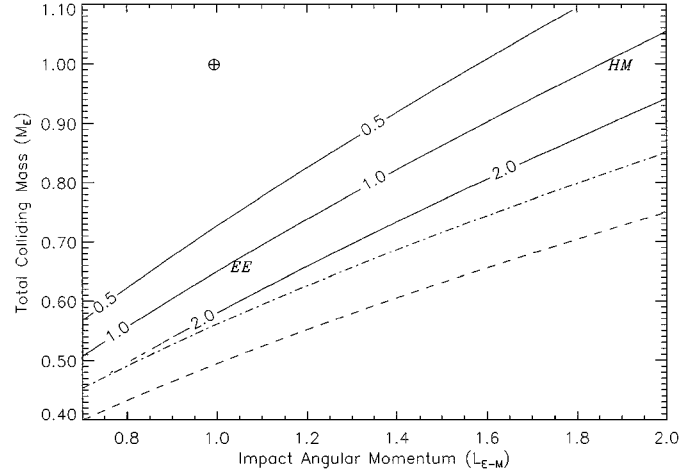


FIG. 4. Contours of the predicted mass of the Moon (shown in lunar masses) that will accrete from an impact-produced disk as a function of colliding mass and angular momentum. The contours were derived from power-law fits to impact experiment data by Cameron (see text) for collisions with impactor to target mass ratios of 3:7. Below a given curve, the predicted moon mass is larger than the specified value until this increase is truncated by the grazing boundary (dashed line). The dot-dashed curve corresponds to $(L/L_*) = 0.9$; between this curve and the grazing limit, simulated disks contain fractions of iron that typically exceed the upper limit on the fraction of the Moon’s mass contained in its core. The Earth symbol corresponds to the coordinate of the current mass and angular momentum of the Earth–Moon system. The early-Earth and high angular momentum impacts, previously shown capable of generating sufficiently massive protolunar disks, are indicated by *EE* and *HM* respectively.

produced disks as a function of (M_T/M_\oplus) and (L/L_{EM}) . Here we have again restricted consideration to $0.5 < (L/L_*) < 1.00$, the range of validity of our power-law fits, and have assumed $a_M = 3.5R_\oplus$ (e.g., Canup and Esposito 1996, Ida *et al.* 1997). Below and to the right of a given contour in Fig. 4, the predicted moon mass is larger than the specified value until this increase is truncated by the grazing boundary (dashed curve).⁴ The basic nature of both the “high angular momentum” (HM) and “early-Earth” (EE) impact classes discussed in Cameron (1997, 2000a,b) and Cameron and Canup (1998) are easily distinguished. The dot-dashed line in Fig. 4 corresponds to the $(L/L_*) = 0.9$ contour; results in Fig. 3 imply that between this line and the grazing limit, impact-generated disks could contain proportionally too much iron to yield the Moon.

From the contours shown in Fig. 4, it appears that impacts other than those simulated to date may also yield a lunar-mass Moon, in particular those involving a total mass $\sim 0.8\text{--}0.9M_\oplus$ and an impact angular momentum $\sim 1.3\text{--}1.5L_{EM}$. Such impacts may represent less restrictive alternatives to previously studied scenarios.

⁴ The grazing boundary is the maximum impact angular momentum obtainable for a $p = (R_M + R_m)$ impact with a given total colliding mass (again assuming zero velocity at infinity and a 3:7 mass ratio between impactor and target).

DISCUSSION

A simple scaling relationship has been identified that describes the results of a recent suite of 41 SPH simulations of potential Moon-forming impacts (Cameron 2000a,b, Cameron and Canup 1998) as a function of nondimensional parameters. Here we do not attempt to explain the physical basis for the functional form but only demonstrate the commonality of outcomes when examined with respect to these scaled quantities. In general, the highest percentage of mass placed into bound orbit is achieved when the impact is slightly less than grazing, which for the 7:3 case implies an angular momentum approximately equal to the maximum angular momentum for rotational stability for a single body with the total system mass, i.e., $L \approx L_*$. The derived maximum yield of material placed into bound orbit is about 4% of the total colliding mass. This suggests that forming Charon (with approximately 12% of Pluto's mass) via a giant impact event may require a quite different sort of impact (e.g., $v > v_{esc}$) than the Moon-forming event and/or that collisions between icy outer solar system bodies are not well characterized by extrapolation from the present lunar-forming simulations.

An interesting feature of Fig. 4 is that the point representative of the current state of the Earth–Moon system lies well outside the contour for even a $M_M \geq 0.5M_{Moon}$ satellite. In addition, the plotted contours tend to overestimate the satellite mass obtainable, given that accretion into a single moon with no escaping material is assumed (i.e., Eq. (4)). A single impact does not appear capable of yielding both the final mass and angular momentum of the Earth–Moon system, a basic quandary that has been discussed in numerous previous works (Canup and Esposito 1996, Ida, *et al.* 1997, Cameron 1997, 2000a,b, Cameron and Canup 1998). If we assume that the Moon did in fact form via a large impact event, this finding suggests one or more of the following: (1) the mass and/or angular momentum of the Earth–Moon system had been significantly modified (presumably by a later impact or impacts) subsequent to the lunar-forming event, (2) regions of parameter space not explored in the above surveys could suggest different scaling relationships that would more easily yield the Earth–Moon system, and/or (3) current SPH methods are not yet adequately modeling processes important to the impact event. The first suggestion has key implications for the impact hypothesis, as well as for the early dynamical and geochemical evolution of the Earth–Moon system. Additional SPH simulations with different impactor to target mass ratios and impact velocities—or that consider a pre-impact Earth with an initial spin—could illuminate the potential effect of (2) and help to map out what is almost certainly a complex phase space relationship that here only a slice of which is seen.

It is encouraging to observe that the predicted ejecta yields from simulations done to date appear quite consistent with one another when comparisons are made using scaled values. As a word of caution, we note that the simulations may nonethe-

less lack fidelity as a whole because of some issue inherent to the techniques utilized. One issue of importance in this regard is the potential effect of numerical resolution, although recent comparisons among $N = 10,000$, 20,000, and 100,000 particle simulations suggest variations in the predicted ejected mass of only ~ 10 –20%. Another possibility is that the equation of state (ANEOS) used to date inadequately treats vaporization. In this regard, it has been pointed out (J. Melosh, personal communication) that the standard version of ANEOS treats all vapor species as monatomic gases, leading to an overestimation of entropy and an underestimation of the amount of vapor produced. The primary emplacement mechanism observed in the simulations discussed here is gravitational torquing caused by interactions among the ejecta fragments and the distorted protoearth, rather than accelerations caused by gas-pressure gradients. Recently, an improvement to ANEOS has been made (B. Pierazzo and J. Melosh, personal communication) which allows for the treatment of molecular vapor. It will be of great interest to determine if simulations utilizing this new version of ANEOS produce results in keeping with the basic relationship discussed here.

APPENDIX A

The post-impact disk mass and angular momentum are dynamic quantities whose values change with time as a result of the disk's viscous evolution. Thus a reference time must be defined when computing and comparing these quantities. Here we have examined the results of impact simulations at characteristic times of 1–2 days after the impact event.⁵

To determine the mass and angular momentum of the bound disk produced around an oblate protoearth in each impact simulation an iterative procedure is utilized. We begin with a data file from a given simulation containing the positions and velocities of all SPH particles in the center-of-mass frame at the time step to be considered. Initial guesses are made for the total mass contained in the post-impact protoearth, M_{PE} , and the protoearth's oblateness or flattening, f , defined by

$$f = \frac{a - b}{a}, \quad (\text{A1})$$

where a and b are the equatorial and polar radii, respectively. The mass of an oblate spheroid protoearth of mean density ρ is

$$M_{PE} = 4\pi a^2 b \rho / 3. \quad (\text{A2})$$

Equations (A1) and (A2) are used to calculate the equatorial radius of the protoearth, a , assuming a terrestrial bulk protoearth density. Orbital elements for particles exterior to a are calculated, and those on bound orbits with periaapses greater than a are considered to be part of the disk.

The mass and angular momentum of the disk particles, together with those of any unbound/escaping particles, are then used to calculate a new estimate for M_{PE} and f . The latter is computed by first determining the angular momentum contained in the protoearth's rotation and the corresponding rotational period,

⁵ SPH simulations depicting the later evolution of the $N = 100,000$ particle simulations are discussed in Cameron (2000b).

T_{PE} , and using this to calculate a new value for the flattening coefficient (e.g., Kaula 1968), where

$$f = \frac{5}{2} \left(\frac{T_*}{T_{PE}} \right)^2 \left/ \left[1 + \left(\frac{5}{2} - \frac{15K}{4} \right)^2 \right] \right., \quad (\text{A3})$$

where T_* is the minimum period for rotational stability from Eq. (1). This value of f , together with the new estimate for M_{PE} , is then used to compute a new a . An improved estimate for the disk mass and angular momentum is then obtained by recalculating the orbital elements of particles exterior to a using the new values for a and M_{PE} . The iteration is continued until convergence is achieved.

We note that the scaling relationships presented here are not particularly sensitive to the specific method used to define the disk mass. A simpler method that assumed a spherical protoearth with radius $R = (M_T / (4/3\pi\rho))^{1/3}$ produced somewhat different values for individual disk masses and angular momenta but yielded scaling relations that were nearly indistinguishable from those in Fig. 2.

APPENDIX B

To relate the scaled angular momentum to the impact parameter for an impact with zero energy at infinity, we use relationships for the conservation of momentum in the rest frame of the center of mass, conservation of angular momentum, conservation of energy, and impact parameter. These are

$$MV + mv = 0, \quad (\text{B1})$$

$$L = mvp_m - MVp_M, \quad (\text{B2})$$

$$E = \frac{1}{2}MV^2 + \frac{1}{2}mv^2 - \frac{GMm}{R_M + R_m} = 0, \quad (\text{B3})$$

$$p = p_M + p_m = (R_M + R_m) \sin \xi, \quad (\text{B4})$$

where the uppercase notation refers to the target and the lowercase to the projectile.

From (B1) and (B2), $L = mvp$; while from (B1) and (B3), $mv = \sqrt{2\mu GMm / (R_M + R_m)}$, with $1/\mu = 1/M + 1/m$ being the so-called reduced mass. Combining with (B4), we find

$$L = \gamma(1 - \gamma)M_T \sqrt{2GM_T(R_M + R_m)} \sin \xi, \quad (\text{B5})$$

where $M_T \equiv M + m$, $\gamma \equiv m/M_T$. Dividing (B5) by Eq. (1) from the text then gives

$$\frac{L}{L_*} = \frac{\sqrt{2}}{K} \gamma(1 - \gamma) \sqrt{\frac{R_M + R_m}{R_T}} \sin \xi. \quad (\text{B6})$$

Finally, if we assume that the target and projectile have the same average density, $R_m/R_T = \gamma^{1/3}$, $R_M/R_T = (1 - \gamma)^{1/3}$, and (B6) reduces to Eq. (2).

ACKNOWLEDGMENTS

We thank W. Benz and an anonymous reviewer for their constructive suggestions. This work has been supported by NASA's Origins of Solar Systems and NSF's Life in Extreme Environments programs.

REFERENCES

- Agnor, C. B., R. M. Canup, and H. F. Levison 1999. On the character and consequences of large impacts in the late stage of terrestrial planet formation. *Icarus* **142**, 219–237.
- Benz, W., W. L. Slattery, and A. G. W. Cameron 1986. The origin of the Moon and the single impact hypothesis I. *Icarus* **66**, 515–535.
- Benz, W., W. L. Slattery, and A. G. W. Cameron 1987. The origin of the Moon and the single impact hypothesis II. *Icarus* **71**, 30–45.
- Benz, W., A. G. W. Cameron, and H. J. Melosh 1989. The origin of the Moon and the single impact hypothesis III. *Icarus* **81**, 113–131.
- Cameron, A. G. W. 1997. The origin of the Moon and the single impact hypothesis V. *Icarus* **126**, 126.
- Cameron, A. B. W. 2000a. Higher-resolution simulations of the giant impact. In *Origin of the Earth and Moon* (R. M. Canup and K. Righter, Eds.), pp. 133–144. Univ. Arizona Press, Tucson.
- Cameron, A. G. W. 2000b. From interstellar gas to the Earth–Moon system. To appear in *Meteorol. Planet. Sci.*
- Cameron, A. G. W. and W. Benz 1991. The origin of the Moon and the single impact hypothesis IV. *Icarus* **92**, 204–216.
- Cameron, A. G. W., and R. M. Canup 1998. The giant impact occurred during Earth accretion. *Lunar Science XXIX*, CD-ROM.
- Cameron, A. G. W., and W. R. Ward 1976. The origin of the Moon. *Proc. Lunar Sci. Conf. 7th*, 120–122.
- Canup, R. M. and L. W. Esposito 1996. Accretion of the Moon from an impact-generated disk. *Icarus* **119**, 427–446.
- Halliday, A. N., D.-C. Lee, and S. B. Jacobsen 2000. Tungsten isotopes, the timing of metal-silicate fractionation, and the origin of the Earth and Moon. In *Origin of the Earth and Moon* (R. M. Canup and K. Righter, Eds.), pp. 45–62. Univ. Arizona Press, Tucson.
- Hartmann, W. K., and D. R. Davis 1975. Satellite-sized planetesimals and lunar origin. *Icarus* **24**, 504–515.
- Hood, L. L., and M. T. Zuber 2000. Recent refinements in geophysical constraints on lunar origin and evolution. In *Origin of the Earth and Moon* (R. H. Canup and K. Righter, Eds.), pp. 397–409. Univ. of Arizona Press, Tucson.
- Ida, S., R. M. Canup, and G. R. Stewart 1997. Lunar accretion from an impact generated disk. *Nature* **389**, 353–357.
- Kaula, W. M. 1968. *Introduction to Planetary Physics: The Terrestrial Planets*. Wiley, New York.
- Kokubo, E., J. Makino, and S. Ida 2000a. Evolution of a circumterrestrial disk and formation of a single Moon. *Icarus*, in press.
- Kokubo, E., R. M. Canup, and S. Ida 2000b. Lunar accretion from an impact-generated disk. In *Origin of the Earth and Moon* (R. M. Canup and K. Righter, Eds.), pp. 145–164. Univ. Arizona Press, Tucson.
- Stewart, G. R. 2000. Outstanding questions for the giant impact hypothesis. In *Origin of the Earth and Moon* (R. M. Canup and K. Righter, Eds.), pp. 217–223. Univ. Arizona Press, Tucson.